

Analysis of Kaon Production at SIS Energies*

E. L. Bratkovskaya, W. Cassing and U. Mosel
Institut für Theoretische Physik, Universität Giessen
35392 Giessen, Germany

Abstract

We analyse the production and propagation of pions and kaons in heavy-ion reactions from 0.8 – 1.8 A·GeV within a coupled channel transport approach including the kaon production channels $BB \rightarrow K^+YN$, $\pi B \rightarrow K^+Y$, $BB \rightarrow N NK\bar{K}$, $\pi B \rightarrow NK\bar{K}$, $K^+B \rightarrow K^+B$ and $\pi\pi \rightarrow K\bar{K}$. Assuming the hyperon selfenergy to be 2/3 of the nucleon selfenergy we find that all inclusive experimental K^+ spectra at SIS energies can be reproduced reasonably well without any selfenergies for the kaons although a slightly repulsive kaon potential cannot be excluded by the present data on kaon spectra and flow.

PACS: 25.75.+r, 13.75 y

Keywords: Relativistic heavy-ion collisions, kaon-baryon interactions

*supported by GSI Darmstadt, BMBF and DFG Graduiertenkolleg

1 Introduction

The study of hadron properties in the dense nuclear medium via relativistic nucleus-nucleus collisions is a major aim of high energy heavy-ion physics. Especially the production of particles at 'subthreshold' energies is expected to provide some valuable insight into the properties of hadrons at high baryon density and temperature [1]. In this respect selfenergy effects in the production of particles have been found previously for antiprotons by a number of groups [2]–[5] though the actual magnitude of the attractive \bar{p} -potential in the nuclear medium is still a matter of debate. Also antikaons according to Refs. [6]–[15] should feel strong attractive forces in the medium whereas the kaon potential is expected to be slightly repulsive at finite baryon density. A first exploratory study with respect to antikaon selfenergies by Li, Ko and Fang in Ref. [16] indicated that sizeable attractive K^- potentials are needed to explain the experimental spectra from [17] for Ni + Ni at 1.85 A·GeV. Indeed, their findings could be substantiated recently in Ref. [18] in a systematic analysis of antikaon production in nucleus-nucleus collisions. So far the production of K^+ mesons has been primarily addressed in order to learn about the incompressibility of the nuclear equation of state [19, 20]. On the other hand, this process could also give information on the predicted repulsive kaon potential. This should also be seen in reduced kaon production yields since at 1 – 2 A·GeV already considerable baryon densities (up to $3 \rho_0 \approx 0.5 \text{ fm}^{-3}$) can be reached in the compression phase [1]. According to the study in Ref. [15] the repulsive kaon potential might be even about 100 MeV at $2\rho_0$ which should lead to a sizeable reduction of the cross section.

The most serious problem related to K^+ production at 'subthreshold' energies are the baryon-baryon elementary production cross sections close to threshold where no experimental data had been available so far and rough extrapolations have been used [21, 22]. Only very recently a new experimental data point has been obtained 2 MeV above the kaon production threshold in pp collisions [23], which can be used for more accurate parametrizations of the elementary production cross section and a systematic reanalysis of the experimental data taken up to now.

Our paper is organized as follows: In Section 2 we briefly describe the transport approach employed as well as the new parametrizations for the elementary strangeness production channels. Section 3 contains a detailed comparison of our calculations with the available data at SIS energies while Section 4 concludes our study with a summary.

2 Model – Ingredients

In this paper we perform our analysis along the line of the HSD¹ approach [24] which is based on a coupled set of covariant transport equations for the phase-space distributions $f_h(x, p)$ of hadron h [24, 25], i.e.

$$\begin{aligned}
& \left\{ \left(\Pi_\mu - \Pi_\nu \partial_\mu^p U_h^\nu - M_h^* \partial_\mu^p U_h^S \right) \partial_x^\mu + \left(\Pi_\nu \partial_\mu^x U_h^\nu + M_h^* \partial_\mu^x U_h^S \right) \partial_p^\mu \right\} f_h(x, p) \\
&= \sum_{h_2 h_3 h_4 \dots} \int d^2 d^3 d^4 \dots [G^\dagger G]_{12 \rightarrow 34 \dots} \delta^4(\Pi + \Pi_2 - \Pi_3 - \Pi_4 \dots) \\
&\times \left\{ f_{h_3}(x, p_3) f_{h_4}(x, p_4) \bar{f}_h(x, p) \bar{f}_{h_2}(x, p_2) \right. \\
&\quad \left. - f_h(x, p) f_{h_2}(x, p_2) \bar{f}_{h_3}(x, p_3) \bar{f}_{h_4}(x, p_4) \right\} \dots \quad .
\end{aligned} \tag{1}$$

In Eq. (1) $U_h^S(x, p)$ and $U_h^\mu(x, p)$ denote the real part of the scalar and vector hadron selfenergies, respectively, while $[G^\dagger G]_{12 \rightarrow 34 \dots} \delta^4(\Pi + \Pi_2 - \Pi_3 - \Pi_4 \dots)$ is the 'transition rate' for the process $1 + 2 \rightarrow 3 + 4 + \dots$ which is taken to be on-shell in the semiclassical limit adopted. The hadron quasi-particle properties in (1) are defined via the mass-shell constraint [25],

$$\delta(\Pi_\mu \Pi^\mu - M_h^{*2}) \quad , \tag{2}$$

with effective masses and momenta (in local Thomas-Fermi approximation) given by

$$\begin{aligned}
M_h^*(x, p) &= M_h + U_h^S(x, p) \\
\Pi^\mu(x, p) &= p^\mu - U_h^\mu(x, p) \quad ,
\end{aligned} \tag{3}$$

while the phase-space factors

$$\bar{f}_h(x, p) = 1 \pm f_h(x, p) \tag{4}$$

are responsible for fermion Pauli-blocking or Bose enhancement, respectively, depending on the type of hadron in the final/initial channel. The dots in Eq. (1) stand for further contributions to the collision term with more than two hadrons in the final/initial channels. The transport approach (1) is fully specified by $U_h^S(x, p)$ and $U_h^\mu(x, p)$ ($\mu = 0, 1, 2, 3$), which determine the mean-field propagation of the hadrons, and by the transition rates $G^\dagger G \delta^4(\dots)$ in the collision term, that describes the scattering and hadron production/absorption rates.

The scalar and vector mean fields U_h^S and U_h^μ for baryons are taken from Ref. [24]; the hyperon selfenergies are assumed to be 2/3 of the nucleon selfenergies as in [24]. In the present approach we propagate explicitly pions, η 's, ρ 's, ω 's and Φ 's as free particles whereas kaons and antikaons are propagated with effective potentials.

¹Hadron String Dynamics

As in case of antiprotons there are several models for the kaon and antikaon selfenergies [6]–[15], which all differ in the actual magnitude of the selfenergies, but agree on the relative signs for kaons and antikaons. Thus in line with the kaon-nucleon scattering amplitude the K^+ potential should be slightly repulsive at finite baryon density whereas the antikaon should see an attractive potential in the nuclear medium. Without going into a detailed discussion of the various models we adopt the more practical point of view, that the actual K^+ selfenergies are unknown and as a guide for our analysis use a linear extrapolation of the form (cf. [18]),

$$m_K^*(\rho_B) = m_K^0 \left(1 + \alpha \frac{\rho_B}{\rho_0} \right), \quad (5)$$

with α describing the strength of the kaon potential at finite baryon density ρ_B . For our following analysis we will restrict to $\alpha = 0$ and $\alpha = 0.06$ to model a slightly repulsive kaon potential. We note that the kaon potential determined from the kaon-nucleon scattering length a_{KN} within the impulse approximation [26] leads to $\alpha \approx 0.06$ when using the isospin averaged scattering length $\bar{a}_{KN} \approx -0.255$ fm from Ref. [27].

First, the individual production channels of the kaons have to be specified. Here, we express the cross sections as a function of the scaled invariant energy squared s_0/s , since the change of the quasi-particle mass then can be incorporated in the threshold energy $\sqrt{s_0}$ for the particular channel. This recipe might be still a matter of debate; our findings in Refs. [28, 29, 30, 31] indicate, that the production is essentially dominated by phase space close to threshold and thus a scaling in s_0/s should be a good approximation.

The isospin averaged production cross section of a $K^+\Lambda$ and $K^+\Sigma$ pair in a nucleon-nucleon collision is related to the measured isospin channels as:

$$\sigma_{NN \rightarrow K^+\Lambda N} = \frac{3}{2} \sigma_{pp \rightarrow K^+\Lambda p} \quad (6)$$

$$\sigma_{NN \rightarrow K^+\Sigma N} = \frac{3}{2} (\sigma_{pp \rightarrow K^0\Sigma^+p} + \sigma_{pp \rightarrow K^+\Sigma^0p}). \quad (7)$$

Following [29] the reaction cross section can be approximated by

$$\sigma_{pp \rightarrow K^+\Lambda p}(s) = 732 \left(1 - \frac{s_{01}}{s} \right)^{1.8} \left(\frac{s_{01}}{s} \right)^{1.5} [\mu b] \quad (8)$$

$$\sigma_{pp \rightarrow K^0\Sigma^+p}(s) = 338.46 \left(1 - \frac{s_{02}}{s} \right)^{2.25} \left(\frac{s_{02}}{s} \right)^{1.35} [\mu b] \quad (9)$$

$$\sigma_{pp \rightarrow K^+\Sigma^0p}(s) = 275.27 \left(1 - \frac{s_{02}}{s} \right)^{1.98} \left(\frac{s_{02}}{s} \right) [\mu b] \quad (10)$$

with $\sqrt{s_{01}} = m_\Lambda - m_N + m_K^0$ and $\sqrt{s_{02}} = m_\Sigma + m_N + m_K^0$. According to isospin relations the $N\Delta$ and $\Delta\Delta$ production channels get additional factors of 3/4 and 1/2, respectively. This scaling of the ΔN and $\Delta\Delta$ production channels from Ref. [22], however, is questionable

and further microscopic studies along the lines of Refs. [32, 33] will be necessary to determine these reaction cross sections more accurately.

The elementary cross sections for the pion induced channels $\pi N \rightarrow K^+ Y$ have been computed by Tsushima et al. in Ref. [34], which we adopt for our present study. K^+ elastic scattering with nucleons also has an impact on the final kaon spectra; the elastic cross section employed is displayed in Fig. 5 of Ref. [18]. In addition, we include the $K\bar{K}$ production channels in baryon-baryon (BB), πB and $\pi\pi$ collisions within the parametrizations from [18] which, however, do not contribute significantly to the inclusive K^+ yield.

The calculation of 'subthreshold' particle production is described in detail in Refs. [1, 35] and has to be treated perturbatively in the energy regime of interest here due to the small cross sections involved. Since we work within the parallel ensemble algorithm, each parallel run of the transport calculation can be considered approximately as an individual reaction event, where binary reactions in the entrance channel at given invariant energy \sqrt{s} lead to final states with 2 (e.g. $K^+ Y$ in πB channels) or 3 (e.g. for $K^+ Y N$ channels in BB collisions) particles with a relative weight W_i for each event i which is defined by the ratio of the production cross section to the total hadron-hadron cross section². The perturbative treatment now implies that in case of strangeness production channels the initial hadrons are not modified in the respective final channel. On the other hand, each strange hadron is represented by a testparticle with weight W_i and propagated according to the Hamilton equations of motion. Elastic and inelastic reactions with pions, η 's or nonstrange baryons are computed in the standard way [1]; however, only the dynamical feedback of the strange hadrons to the nonstrange mesons and baryons is neglected. The final cross section is obtained by multiplying each testparticle with its weight W_i . In this way one achieves a time-saving simulation of the strangeness production, propagation and reabsorption during the heavy-ion collision.

3 Results

Since Δ - and pion-induced channels play a major role for K^+ production, we start our analysis with a comparison of our calculations for pion production at SIS energies with the available π^+ data for Ni + Ni at 1.0 and 1.8 A·GeV and Au + Au at 1.0 A·GeV in Fig. 1. The experimental spectra at $\theta_{lab} = 44^\circ \pm 4^\circ$ [36] are described reasonably well in the whole kinematical range not only for Ni + Ni, but also for Au + Au. We slightly underestimate the pion spectrum for Ni + Ni at 1.8 A·GeV at low momenta which

²The actual final states are chosen by Monte Carlo sampling according to the 2, or 3-body phase space.

might reflect limitations of our configuration space showing up at higher bombarding energy. For future comparison we also include our results for the inclusive π^+ spectra from Au + Au at 1.5 A·GeV (upper histogram). For a more detailed analysis of pion production at SIS energies we refer the reader to Ref. [37], which works in a very similar theoretical framework. For our present purpose we only conclude that the pion and baryon dynamics including the Δ and higher resonance dynamics in our transport calculations are sufficiently well under control.

The Lorentz invariant K^+ spectra for Ni + Ni at 0.8, 1.0 and 1.8 A·GeV from the same calculations as above are shown in Fig. 2 in comparison to the data from [38]. Here the full lines reflect calculations including only bare K^+ masses ($\alpha = 0$) while the dashed lines correspond to calculations with $\alpha = 0.06$ in Eq. (5), which leads to about a 30 MeV increase of the kaon mass at ρ_0 . Note that the repulsive kaon potential from Ref. [15] is best fitted for $\alpha = 0.1$, which would imply a further reduction of the K^+ cross section. When fitting an exponential to the Lorentz invariant spectrum $\sim \exp(-E/T_0)$, where E is the kinetic energy of the kaon in the cms, we obtain slope parameters $T_0 \approx 60$ MeV, 75 MeV and 102 MeV at the bombarding energy of 0.8, 1.0 and 1.8 A·GeV, respectively.

The general tendency seen at all bombarding energies is that our calculations with a bare kaon mass provide a better description of the experimental data for Ni + Ni than those with an enhanced kaon mass. Since this general trend might be accidental we also compare our calculations for the heavier systems, i.e. Bi + Pb at 0.8 A·GeV and Au + Au at 1.0 A·GeV, with the respective experimental data [39, 40, 41] in Fig. 3. The full dots represent the earlier data for Au + Au at 1.0 A·GeV [40] while the open circles result from a new measurement [41] of the system at the same bombarding energy. Both calculations (solid line: $\alpha = 0$; dashed line: $\alpha = 0.06$) are compatible with the data due to the experimental uncertainties. As in case of antikaons [18] the selfenergy effects are most pronounced at low center-of-mass momenta of the kaons where, unfortunately, no data have been taken so far. For future comparison we also include our results for Au + Au at 1.5 A·GeV.

With our new elementary cross sections the relative weights of the K^+ production channels change considerably compared to our earlier calculations [42] as can be seen from Fig. 4 for Au + Au at 1 A·GeV. Whereas the NN production channels (dashed line) are almost negligible as before [42] the dominant yield now stems from πN reactions (dot-dot-dashed line) which surpass the $N\Delta$ channel (dot-dashed line). This change comes about because our old calculations [42] were performed in the so-called frozen- Δ approximation in which the Δ 's are not allowed to decay until the collision has ended. The main message of the old studies, that the secondary reactions are very important for a description of the kaon yield, however, survives. The calculation in Fig. 4 has been

performed for a bare K^+ mass; we note that the relative channel decomposition does not change very much when performing a calculation with a slightly repulsive kaon potential.

In Fig. 5 we present the ratio N_{K^+}/N_{π^+} versus the number of participating nucleons A_{part} – which is a measure of the impact parameter b – from our calculations for Ni + Ni at 1.0 and 1.8 A·GeV as well as for Au + Au at 1.0 and 1.5 A·GeV for $\alpha = 0$ (solid lines) and $\alpha = 0.06$ (dashed lines). The experimental data have been taken from Ref. [40]. The ‘theoretical’ error bars indicate the calculational uncertainty due to the finite particle statistics, since only mesons for $\theta_{lab} = 44^\circ \pm 4^\circ$ have been taken into account. The ratio N_{K^+}/N_{π^+} increases with A_{part} in all cases; this increase is more pronounced at the lower bombarding energy of 1.0 A·GeV and for the heavier system Au + Au. In our calculation this increase in the relative K^+ yield is due to a strong rise in N_{K^+}/A_{part} ; N_{π^+}/A_{part} is flat as a function of A_{part} . Because the kaons are mainly due to the secondary collisions, they are predominantly produced at high baryon density $1.5\rho_0 < \rho_B < 2.5\rho_0$ while the pion production occurs at lower density, too. Since the volume for the high baryon density increases sizeably when going from peripheral to more central collisions, the K^+/π^+ ratio has to increase accordingly. The relative contribution of the various production channels to the total K^+ yield are shown in Fig. 6 as a function of A_{part} for Ni + Ni at 1.0 and 1.8 A·GeV. It can clearly be seen that the relative importance of the primary NN channel increases with energy, but that of the secondary πN reaction decreases. This explains the flatter behavior seen in Fig. 5 for the higher energies.

In Fig. 7 we show the angular distribution of the produced kaons for Au + Au at 1 A·GeV which exhibits a forward-backward peaking. By comparing our calculations with and without angular dependence in the elementary kaon production cross section we have verified that this angular anisotropy is not due to the elementary production processes. Instead, it reflects the forward-backward peaking of the pion angular distribution [37]. The figure shows that the rescattering of the kaons enhances the anisotropy somewhat, but is not solely responsible for it.

A further quantity of interest – in the context of our present analysis – is the kaon flow in the reaction plane, which should show some sensitivity to the kaon potential in the nuclear medium as put forward by Li, Ko and Brown [43, 44, 45, 46] and is presently investigated by the FOPI Collaboration [47, 48]. Here due to elastic scattering with nucleons the kaons partly flow in the direction of the nucleons thus showing a positive flow in case of no mean-field potentials [43]. With increasing repulsive kaon potential the positive flow will turn to zero and then become negative; experimental data on kaon flow thus are expected to discriminate further on the potentials seen in the medium. In order to investigate this question we have performed detailed (and high statistics) calculations for K^+ production in Ni + Ni reactions at 1.93 A·GeV as measured by the FOPI Collaboration

[48]. In order to compare with their data we have included a transverse momentum cut $p_T \geq 0.5 m_K$, where m_K is the kaon mass, and gated on central collisions with impact parameter $b \leq 4$ fm as in Ref. [45]. The results of our calculations are displayed in Fig. 8 in terms of $\langle p_x \rangle / m_K$ versus the normalized rapidity

$$y^0 = \frac{y_{cm}}{y_{proj}}, \quad (11)$$

where y_{cm} and y_{proj} are the kaon and projectile rapidity in the cms, respectively. Our calculations without any kaon potential ($\alpha = 0$, full line) indeed show a positive flow as expected, which appears still to be compatible with the data within the error bars and is practically identical to the respective calculations from Ref. [45]. On the other hand, increasing the kaon potential ($\alpha = 0.06$, dashed line) the kaon flow becomes slightly negative or comparable to zero, quantitatively in line with the calculations from Ref. [45] and in somewhat better agreement with the data. Thus in case of the flow observable a slightly repulsive kaon potential (≈ 30 MeV at ρ_0) is more in line with the present data of the FOPI Collaboration [48].

4 Summary

In this work we have presented a detailed study of pion and kaon production in nucleus-nucleus collisions for medium and heavy systems from 0.8 to 1.8 A·GeV within the coupled channel BUU approach, where the kaons are produced perturbatively, however, propagated explicitly with their final state interactions. An important ingredient of our reanalysis of the kaon cross sections are the novel elementary production cross sections from Refs. [28, 29, 31] and from Ref. [34] for the pion induced channels. We note, however, that the ΔN and $\Delta\Delta$ production channels are not that well determined and require further theoretical efforts.

Our analysis shows that the π^+ spectra are reasonably well described in this energy regime without introducing any medium modifications for these mesons (cf. also Ref. [37]). This is understood in terms of the strong reabsorption of pions that essentially leads to the surface-emission. For the much more penetrating K^+ mesons our results also show no final convincing indications of in-medium changes. The new kaon spectra for the heavy system Au + Au at 1 A·GeV as well as the kaon flow data for Ni + Ni at 1.93 A·GeV can – within their errorbars – be described by assuming free kaon properties although there seems to be a tendency to favor a small repulsive kaon potential of about +30 MeV at normal nuclear matter density, which would be in line with the kaon potential as extracted from the kaon-nucleon scattering length in the impulse approximation [26]. On the other hand, we find that more repulsive kaon potentials as predicted by some Lagrangian models

appear not to be compatible with the available data and in particular with the K^+/π^+ ratios. An upcoming data analysis in the form of Fig. 5 and high statistics data on kaon flow in the form of Fig. 8 should shed some further light on this issue. However, even then theoretical uncertainties connected with our insufficient knowledge of Δ -induced cross sections will remain.

The authors acknowledge valuable and inspiring discussions throughout this work with N. Herrmann, H. Oeschler, P. Senger, A. Sibirtsev and Gy. Wolf.

References

- [1] W. Cassing and U. Mosel, *Prog. Part. Nucl. Phys.* 25 (1990) 235.
- [2] S. Teis, W. Cassing, T. Maruyama, and U. Mosel, *Phys. Lett. B* 319 (1993) 47; *Phys. Rev. C* 50 (1994) 388.
- [3] G. Q. Li, C. M. Ko, X. S. Fang, and Y. M. Zheng, *Phys. Rev. C* 49 (1994) 1139.
- [4] W. Cassing, A. Lang, S. Teis, and K. Weber, *Nucl. Phys. A* 545 (1992) 123c.
- [5] G. Batko, A. Faessler, S.W. Huang, E. Lehmann, and R.K. Puri, *J. Phys. G* 20 (1994) 461.
- [6] G. E. Brown, C. M. Ko, Z. G. Wu, and L. H. Xia, *Phys. Rev. C* 43 (1991) 1881.
- [7] G. E. Brown and M. Rho, *Phys. Rev. Lett.* 66 (1991) 2720.
- [8] D. B. Kaplan and A. E. Nelson, *Phys. Lett. B* 175 (1986) 57.
- [9] G. E. Brown, K. Kubodera, and M. Rho, *Phys. Lett. B* 192 (1987) 273; G. E. Brown, C. M. Ko, and K. Kubodera, *Z. Phys. A* 341 (1992) 301.
- [10] C. H. Lee, G. E. Brown, D. P. Min, and M. Rho, *Nucl. Phys. A* 585 (1995) 401.
- [11] G. Q. Li and C. M. Ko, *Phys. Lett. B* 338 (1994) 118.
- [12] M. Rho, 'International Nuclear Physics Conference', Aug. 1995, Beijing, China, to appear in *Nucl. Phys. A*.
- [13] M. Lutz, A. Stein and W. Weise, *Nucl. Phys. A* 574 (1994) 755.
- [14] T. Waas, N. Kaiser, and W. Weise, *Phys. Lett. B* 365 (1996) 12.
- [15] T. Waas, N. Kaiser, and W. Weise, *Phys. Lett. B* 379 (1996) 34.

- [16] G. Q. Li, C. M. Ko, and X. S. Fang, Phys. Lett. B 329 (1994) 149.
- [17] A. Schröter et al., Z. Phys. A 350 (1994) 101.
- [18] W. Cassing, E.L. Bratkovskaya, U. Mosel, S. Teis and A. Sibirtsev, Nucl. Phys. A 614 (1997) 415.
- [19] J. Aichelin, Phys. Reports 202 (1991) 233.
- [20] T. Maruyama, W. Cassing, U. Mosel, S. Teis, and K. Weber, Nucl. Phys. A 573 (1994) 653.
- [21] B. Schürmann and W. Zwermann, Phys. Lett. B 183 (1987) 31.
- [22] J. Randrup and C. M. Ko, Nucl. Phys. A 343 (1980) 519; A 411 (1983) 537.
- [23] J.T. Balewski et al., Phys. Lett. B 388 (1996) 859.
- [24] W. Ehehalt and W. Cassing, Nucl. Phys. A 602 (1996) 449.
- [25] K. Weber, B. Blättel, W. Cassing, H.-C. Dönges, V. Koch, A. Lang, and U. Mosel, Nucl. Phys. A 539 (1992) 713.
- [26] G.E. Brown, C.-H. Lee, M. Rho and V. Thorsson, Nucl. Phys. A 567 (1994) 937.
- [27] T. Barnes and E.S. Swanson, Phys. Rev. C 49 (1994) 1166.
- [28] A. Sibirtsev, H. Müller, C. Schneidereit, and M. Büscher, Z. Phys. A 351 (1995) 333.
- [29] A. Sibirtsev, Phys. Lett. B 359 (1995) 29.
- [30] G. I. Lykasov, M. V. Ryzjanin and W. Cassing, Phys. Lett. B 387 (1996) 691.
- [31] A. Sibirtsev, W. Cassing, and U. Mosel, nucl-th/9607047, Z. Phys. A, in print.
- [32] G.Q. Li and C.M. Ko, Nucl. Phys. A 594 (1995) 439.
- [33] W. Peters, U. Mosel, and A. Engel, Z. Phys. A 353 (1995) 333.
- [34] K. Tsushima, S. W. Huang, and A. Faessler, J. Phys. G 21 (1995) 33; Phys. Lett. B 337 (1994) 245.
- [35] W. Cassing, V. Metag, U. Mosel, and K. Niita, Phys. Rep. 188 (1990) 363.
- [36] C. Müntz et al., Z. Phys. A 352 (1995) 17; D. Brill et al., Z. Phys. A 357 (1997) P 207.

- [37] S. Teis, W. Cassing, M. Effenberger, A. Hombach, U. Mosel, and Gy. Wolf, *Z. Phys. A* 356 (1997) 421.
- [38] P. Senger for the KaoS Collaboration, *Acta Physica Polonica B* 27 (1996) 2993.
- [39] P. Senger et al., Proceedings of the International Workshop XXIII on Gross Properties of Nuclei and Nuclear Excitations, Hirschegg, Austria, January, 1995, p. 306.
- [40] D. Miskowiec, W. Ahner, R. Barth et al., *Phys. Rev. Lett.* 72 (1994) 3650.
- [41] P. Senger, private communication.
- [42] A. Lang, W. Cassing, U. Mosel, and K. Weber, *Nucl. Phys. A* 541 (1992) 507.
- [43] G. Q. Li, C.M. Ko and B.A. Li, *Phys. Rev. Lett.* 74 (1995) 235.
- [44] G.Q. Li and C.M. Ko, *Nucl. Phys. A* 594 (1995) 460.
- [45] G.E. Brown, C.M. Ko and G.Q. Li, nucl-th/9608039.
- [46] G.Q. Li and C.M. Ko, *Phys. Rev. C* 54 (1996) R2159.
- [47] J.L. Ritman et al., *Z. Phys. A* 352 (1995) 355.
- [48] N. Herrmann, *Nucl. Phys. A* 610 (1996) 49c.

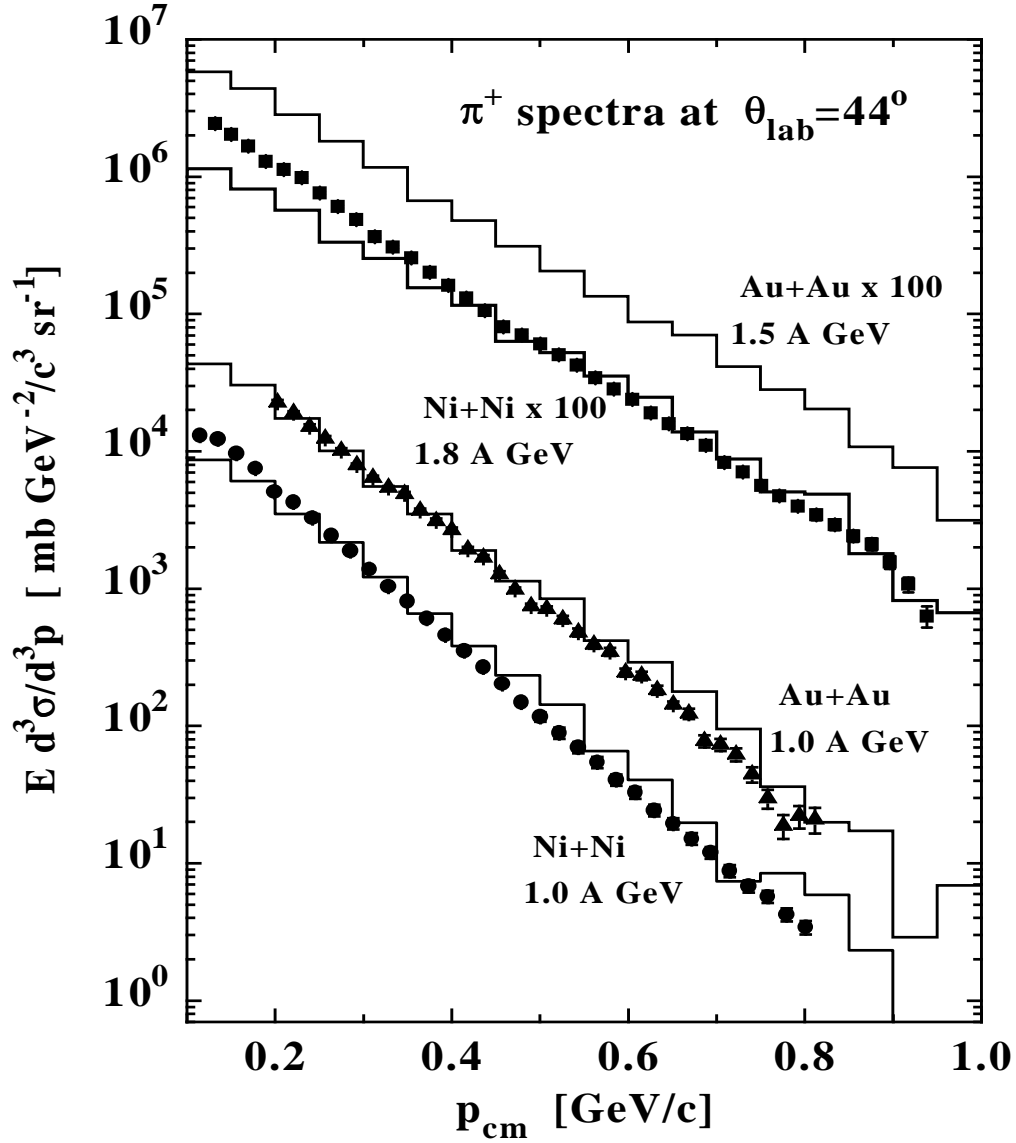


Figure 1: Inclusive π^+ spectra from Ni + Ni collisions at 1.0 and 1.8 A·GeV and Au + Au at 1.0 A·GeV in comparison to the experimental data from Ref. [36] at $\theta_{lab} = 44^\circ \pm 4^\circ$. The upper solid histogram displays our calculations for Au + Au at 1.5 A·GeV .

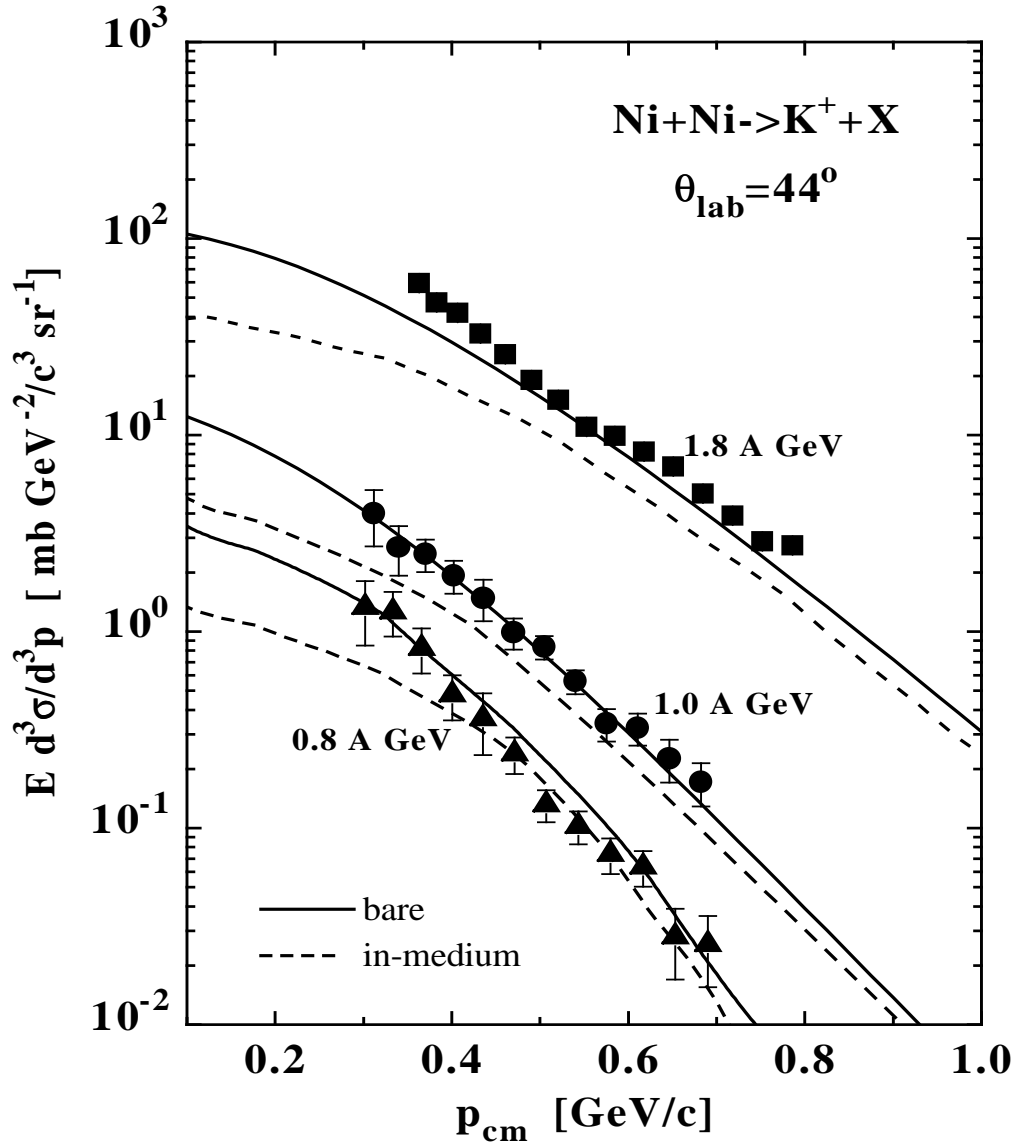


Figure 2: Inclusive K^+ spectra from Ni + Ni collisions at 0.8, 1.0 and 1.8 A·GeV in comparison to the experimental data from Ref. [38] at $\theta_{lab} = 44^\circ \pm 4^\circ$. The solid lines represent calculations with bare K^+ masses, while the dashed lines result for $\alpha = 0.06$ in Eq. (5).

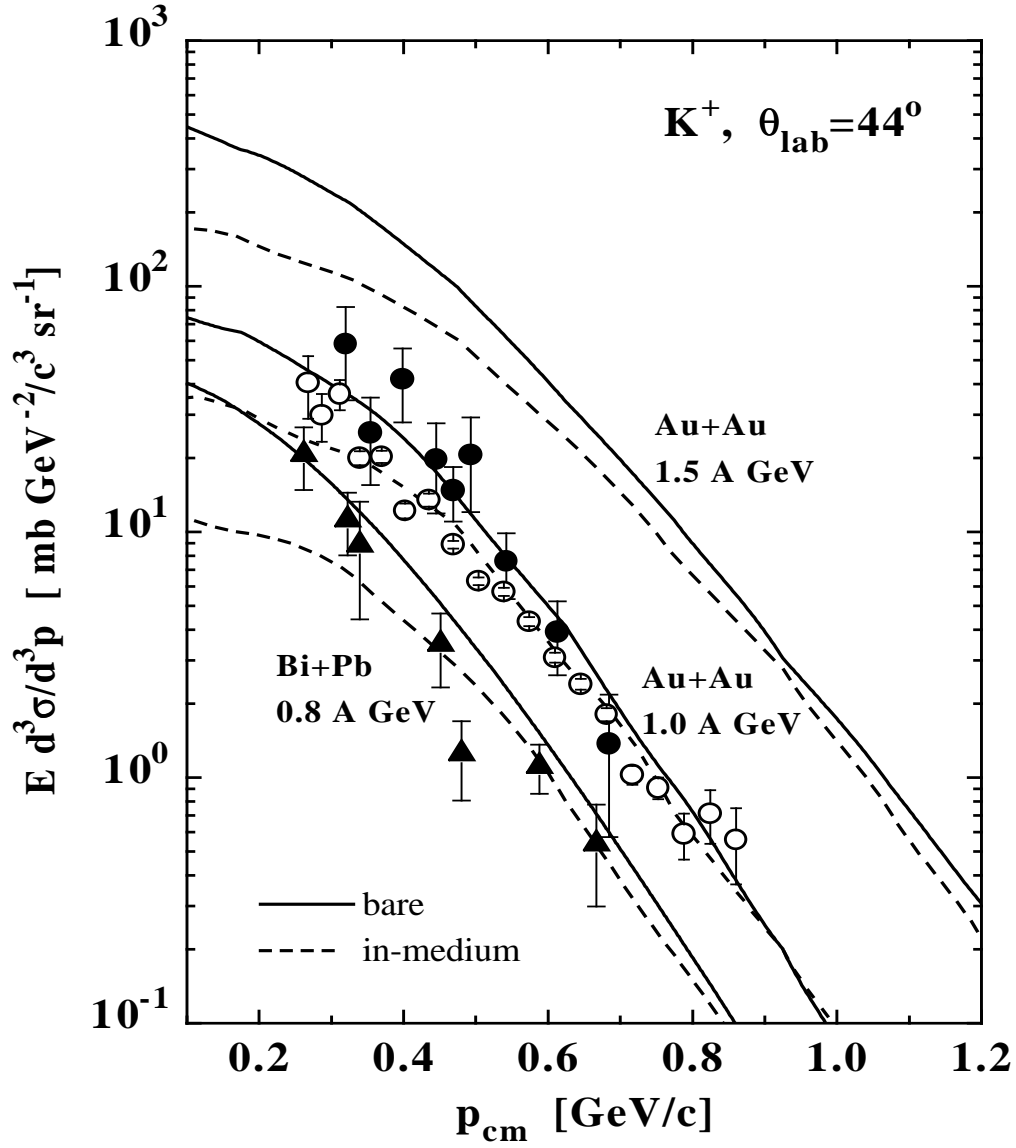


Figure 3: Inclusive K^+ spectra from Bi + Pb collisions at 0.8 A·GeV and Au + Au at 1.0 A·GeV in comparison to the experimental data from Ref. [39, 40, 41] at $\theta_{lab} = 44^\circ \pm 4^\circ$. The solid lines represent calculations with bare K^+ masses, while the dashed lines result for $\alpha = 0.06$ in Eq. (5). The calculations for Au + Au at 1.5 A·GeV are included for future comparison.

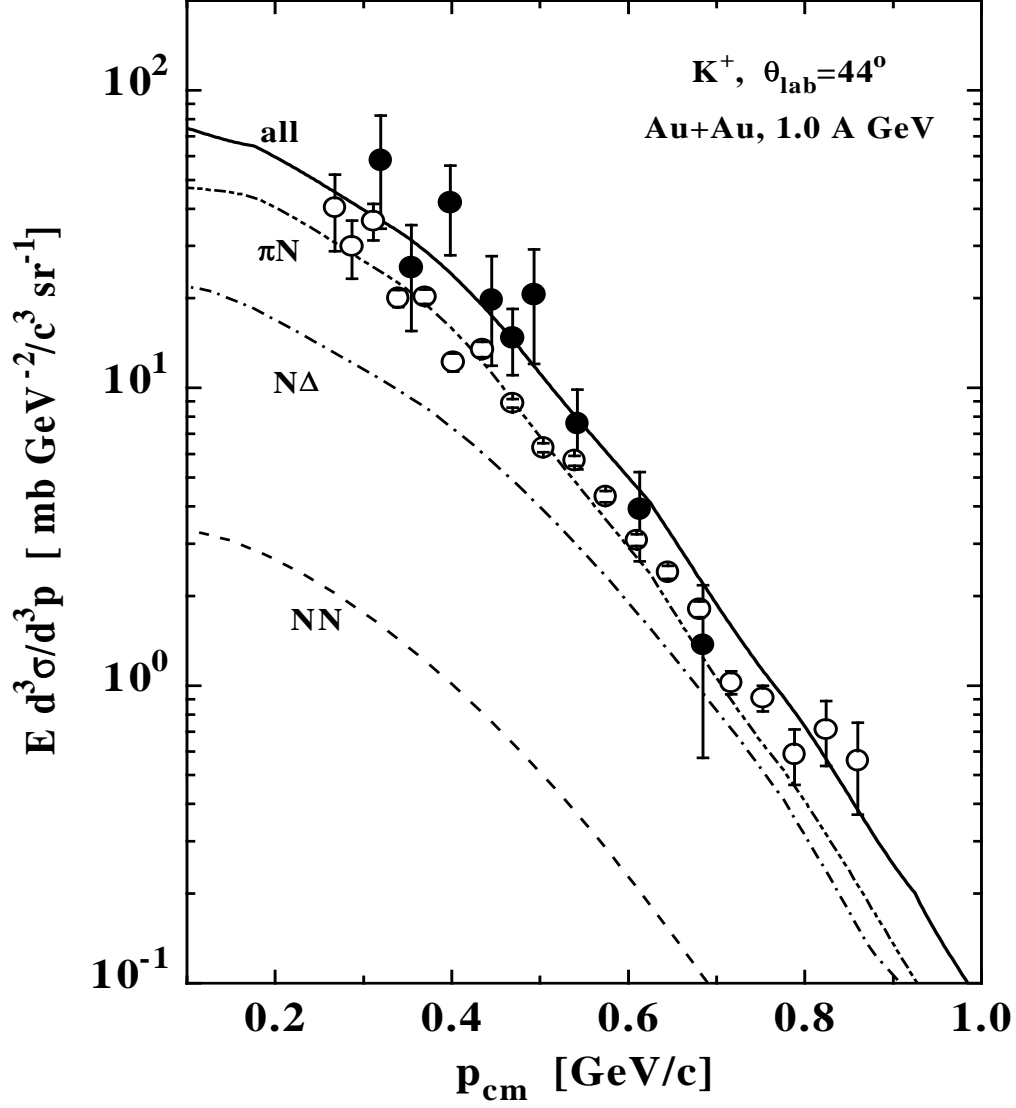


Figure 4: Inclusive K^+ spectra from Au + Au collisions at 1.0 A·GeV (solid line) in comparison to the experimental data from Ref. [40, 41] at $\theta_{lab} = 44^\circ \pm 4^\circ$ for the bare kaon mass scenario. The dashed line represents the contribution from NN collisions while the dot-dashed and dot-dot-dashed line show the contributions from ΔN and πN collisions, respectively.

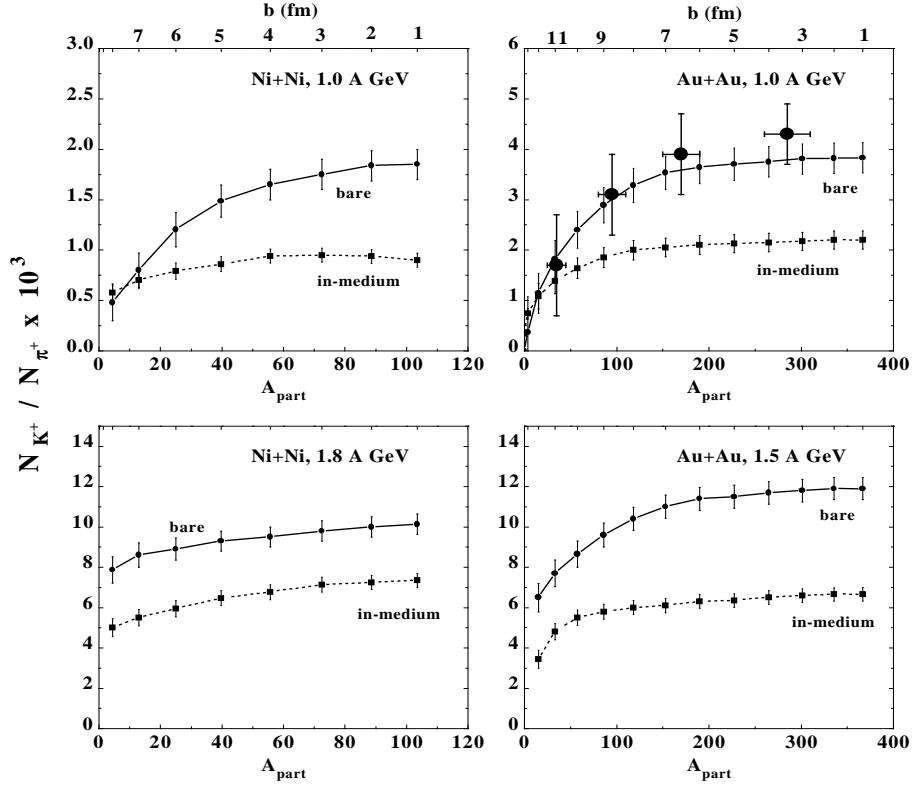


Figure 5: The K^+/π^+ ratio for Ni + Ni at 1.0 and 1.8 A·GeV and Au + Au at 1.0 and 1.5 A·GeV as a function of the number of participating nucleons A_{part} as defined in Ref. [40]. The solid lines represent calculations with bare K^+ masses, while the dashed lines result for $\alpha = 0.06$ in Eq. (5). The experimental data have been taken from Ref. [40].

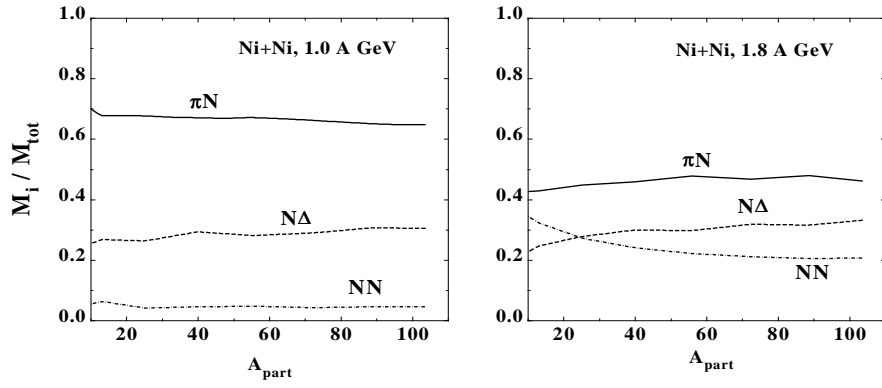


Figure 6: The relative contribution of the various production channels to the total K^+ yield as a function of A_{part} for Ni + Ni at 1.0 and 1.8 A·GeV . The solid line represents the contribution from πN collisions while the dashed and dot-dashed lines show the contributions from ΔN and NN collisions, respectively.

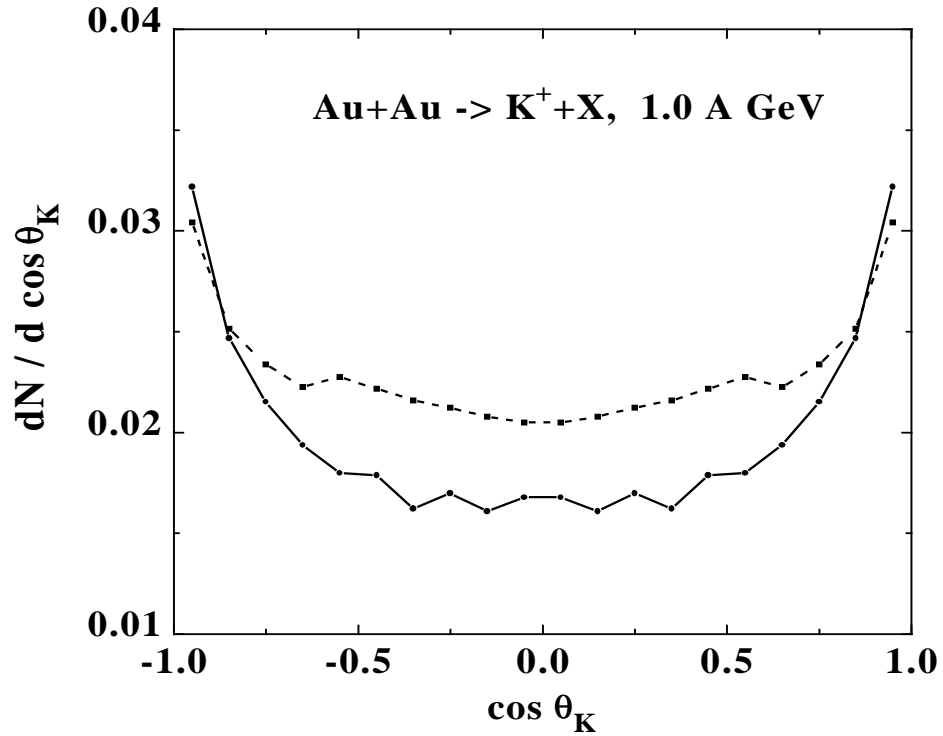


Figure 7: Angular distribution of kaons in the nucleus-nucleus cms for Au + Au collisions at 1 A·GeV including all impact parameters. The dashed line represents a calculation without K^+N rescattering while the solid line shows the results when including kaon rescattering.

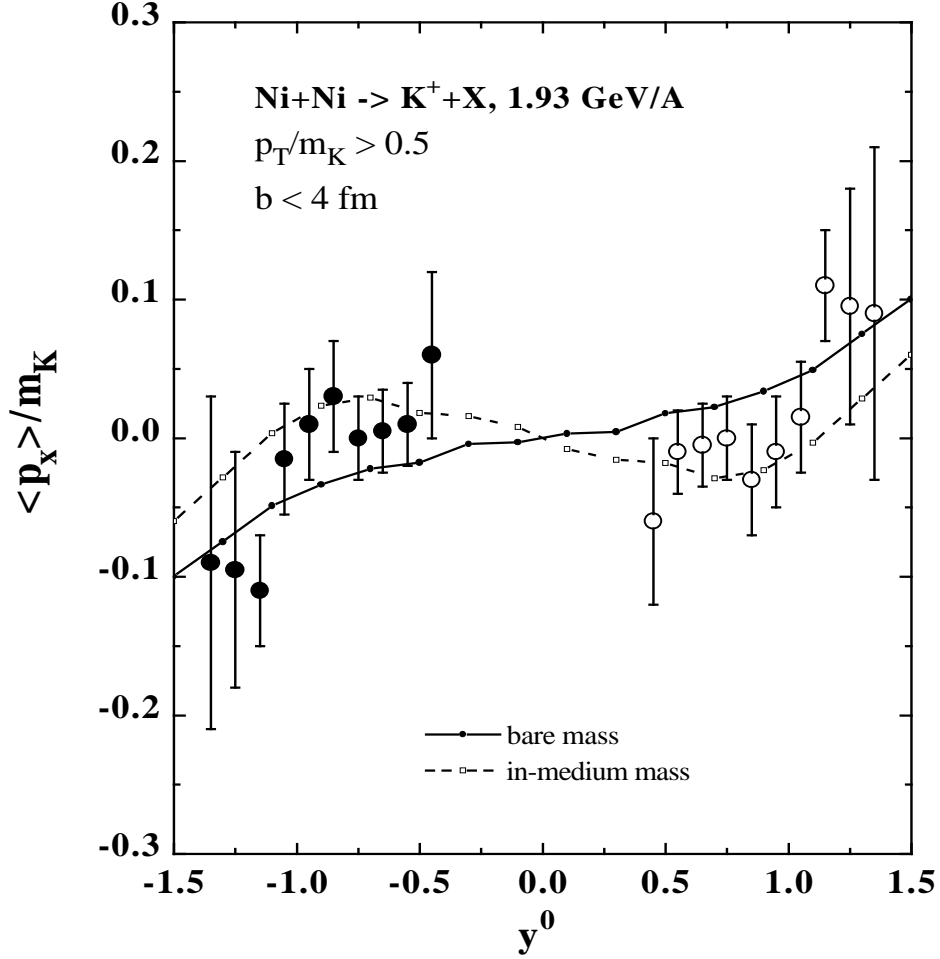


Figure 8: Kaon flow in the reaction plane ($\langle p_x \rangle / m_K$) as a function of the normalized rapidity $y^0 = y_{cm}/y_{proj}$ for Ni + Ni at 1.93 A GeV. We have gated on central collisions ($b \leq 4$ fm) and applied a transverse momentum cut for $p_T \geq 0.5 m_K$ as for the experimental data of the FOPI Collaboration [48] (full dots). The open dots are obtained by reflection at $y^0 = 0$. The solid line and dashed line display the results of our transport calculations without ($\alpha = 0$) and with a slightly repulsive kaon potential ($\alpha = 0.06$), respectively.